Atmospheric oxidation capacity in Chinese megacities during photochemical polluted season: radical budget and secondary pollutants formation

Zhaofeng Tan[1,2], Keding Lu[1]*, Meiqing Jiang[1], Rong Su[1], Hongli Wang[3], Shengrong Lou[3], Qingyan Fu[4], Chongzhi Zhai[5], Qinwen Tan[6], Dingli Yue[7], Duohong Chen[7], Zhanshan Wang[8], Shaodong Xie[1], Limin Zeng[1] & Yuanhang Zhang[1,9]*

[1] State Key Joint Laboratory of Environmental Simulation and Pollution Control, College of Environmental Sciences and Engineering, Peking University, Beijing 100871, China;
[2] Institute of Energy and Climate Research, IEK-8: Troposphere, Forschungszentrum Jülich GmbH, Jülich, Germany
[3] State Environmental Protection Key Laboratory of Formation and Prevention of the Urban Air Complex, Shanghai Academy of Environmental Sciences, Shanghai 200233, China;
[4] Shanghai Environmental Monitoring Center, Shanghai 200235, China;
[5] Ecological and Environmental Monitoring Center of Chongqing, Chongqing 401147, China;
[6] Chengdu Academy of Environmental Sciences, Chengdu 610072, China;
[7] State Environmental Protection Key Laboratory of Regional Air Quality Monitoring, Guangdong Environmental Monitoring Center, Guangzhou 510308, China;
[8] Beijing Key Laboratory of Atmospheric Particulate Monitoring Technology, Beijing Municipal Environmental Monitoring Center, Beijing 100048, China
[9] Beijing Innovation Center for Engineering Sciences and Advanced Technology, Peking University, 100871, Beijing, China

Correspondence to: *k.lu@pku.edu.cn; yhzhang@pku.edu.cn*

Abstract. Atmospheric oxidation capacity is the core of converting freshly-emitted substances to secondary pollutants. In this study, we present in-situ measurements at four Chinese megacities (Beijing, Shanghai, Guangzhou, and Chongqing) during photochemical polluted seasons. The atmospheric oxidation capacity is evaluated using an observational-based model with the input of radical chemistry precursor measurements. The radical budget analysis illustrates the importance of HONO and HCHO photolysis, which contribute nearly half of the total primary radical sources. The radical propagation is efficient due to abundant NO in the urban environments. Hence, the production rate of secondary pollutants, i.e. ozone and fine particle precursors (H_2SO_4, HNO_3, and extreme low volatile organic compounds (ELVOCs)) is fast, resulting in secondary air pollution. The ozone budget demonstrates that strong ozone production occurs in the urban areas, which results in fast ozone concentration increases locally and through transport in downwind areas. The O_3-NO_x-VOC sensitivity tests show that ozone production is VOC-limited and that alkenes and aromatics should be first mitigated for ozone pollution control in the four megacities investigated. In contrast, NO_x emission control will lead to more severe ozone pollution due to the decrease of NO_x. For fine particle pollution, the role of HNO_3-NO_3- partitioning system is investigated with a thermal dynamic model (ISORROPIA2) due to the importance of particulate nitrate during photochemical polluted seasons. The strong nitric acid production converts efficiently to nitrate particles due to high RH and ammonia-rich conditions during photochemical polluted seasons. This study highlights the efficient radical chemistry that maintains the atmospheric oxidation capacity in Chinese megacities, which results in secondary pollution characterized by ozone and fine particles.

1. Introduction

Air pollution is the one of the major threat to human health in cities (Kan et al., 2012). In China, the rapid economic development accompanied by degradation of air quality for the last decades in the eastern areas (Chan and Yao, 2008). More than 300 million

Atmospheric
Chemistry
and Physics
Discussions

people live in the North China Plain (NCP), Yangtze River Delta (YRD) and Pearl River Delta (PRD) regions in eastern China. Among all, Beijing, Shanghai, and Guangzhou are the metropolitan cities in these regions and suffering from severe air pollution. To improve the air quality, emission mitigations have been conducted since the 2000s. As a result, the primary pollutant concentrations decline since then. However, secondary pollution characterized by ozone and fine particle has become the major

5   contributor to air pollution. The major composition of fine particles are secondary components (Tie et al., 2013;Sun et al., 2006;Huang et al., 2014;Guo et al., 2014;Cheng et al., 2016;Zheng et al., 2005;He et al., 2001;Sun et al., 2004), e.g. sulfate, nitrate, and oxidized organic aerosol. This indicates high oxidation capacity in the Chinese pollution environments. The national-wide measurements showed ozone is the only one out of six air quality index substance that increases in the last five years. Therefore, it's difficult to control secondary pollution given the non-linear relation between primary and secondary pollutants. After all,

10   atmospheric oxidation capacity is the key factor that converts primary pollutants to secondary ones. Therefore, it requires the knowledge of the role oxidation processes on the secondary pollution formation.

So far, only limited studies have been performed in China to elucidate the oxidation processes (Lu et al., 2018). The studies in 2006 found an OH source is missing in the current chemical mechanism for low NO_x conditions (Lu et al., 2012;Hofzumahaus et al., 2009;Lu et al., 2013). The study in Wangdu (summer) and Beijing (winter) found an evidence of missing RO_2 sources, which

15   could lead to strong underestimation of ozone production (Tan et al., 2017;Tan et al., 2018c). The radical observation and model comparisons highlight the uncertainty of the radical chemistry in China. The nitrous acid (HONO) were measured and constraint to the model in these studies, which were the major source of the $OH-HO_2-RO_2$ radical system. However, the majority of HONO sources is unclear so far (Su et al., 2011;Ye et al., 2016;Li et al., 2014b). On the other hand, the large aerosol content offers a large surface to conduct heterogeneous reactions. Radical loss on the aerosol surface could also play a role, which is not well understood

20   due to the limited information based on the Chinese aerosol composition. The Chlorine chemistry is gaining increasing attention recently, which acts as a radical source and source of particulate nitrate formation (Tham et al., 2016;Wang et al., 2016;Wang et al., 2017b;Wang et al., 2017c;Wang et al., 2017a). However, the large variability of uptake coefficient and $ClNO_2$ yield adds large uncertainty to heterogeneous reactions (Xue et al., 2014;Tham et al., 2018).

With respect to secondary formation, the radical chemistry is insightful to reveal the key processes. The ozone production rate can

25   be determined by the oxidation rate of NO by HO_2 and RO_2 directly. The gas phase oxidation produced semi- and/or low volatile compounds, which are important precursors for particle formation. Sulfate, nitrate, and SOA are dominant contributors to the particle during heavy polluted episodes (haze events), all of which could be produced in the OH-initiated oxidation processes.

The Chengdu-Chongqing city group (population 90 million) locates in Sichuan Basin (SCB), southwest of China, representing the developing city clusters. Although the new city clusters also suffer from air pollution, only sparse researches have been conducted

30   in these regions, especially for the secondary pollution formation. For the SCB region, only limited studies have been performed regarding the oxidation capacity. Chengdu is evaluated using an observational-based model which found similar radical concentration and ozone production rate (Tan et al., 2018b). The VOC and ozone formation is evaluated in Chongqing (Su et al., 2018;Li et al., 2018b).

In this study, we present the measurement at four megacities, Beijing, Shanghai, Guangzhou, and Chongqing. The focus of this

35   study is to illustrate the atmospheric oxidation processes in the urban areas. The observation periods were selected in typical photochemical polluted seasons to explore the photochemistry and secondary pollution formation. An observational-based model is used to explore the oxidation capacity from the aspect of radical chemistry. This study aims to provide insight into the secondary pollution formation in Chinese megacities. With the intention to illustrate the common feature of the megacities oxidation capacity, we compared the results from different studies. Two questions need to be addressed in this study. First, what is the oxidation

40   capacity in these megacities and which source(s) sustain it? Especially the comparison of city centers to suburban and rural

locations, to foreign countries. Second, what is the secondary formation rate, e.g. ozone and nitrate? What is the limiting factor in secondary pollution formation? Finally, the diagnosis of atmospheric oxidation capacity and secondary pollution formation could provide fundamental knowledge for further air pollution control in China.

2. Methods

2.1 Measurement sites

5

This study presents the measurements at four Chinese megacities, namely Beijing, Shanghai, Guangzhou, and Chongqing. These cities were located in the highly polluted region (Fig. 1). Beijing, Shanghai, and Guangzhou are the main cities in North China Plain (NCP), Yangtze River Delta (YRD), and Pearl River Delta (PRD), which are representative of the most developed region in China. Chongqing is one of the biggest cities in southwestern China (population of 30 million), representing the Chinese developing

10 city clusters.

The detail of the field campaigns is summarized in Table 1. All measurements sites locate within the city downtown areas to represent the conditions in the city center. Beijing is located on the north edge of the North China Plain and is the most north station (39.9 °N) than others. The campaigns were mainly conducted in summer to represent the most active photochemical season. The Beijing campaign took place in mid-summer (June) and thus the strongest solar radiation input. The latitude of Shanghai (31.1 °N)

15 and Chongqing (29.6 °N) are similar as well as the observation period (August). Therefore, the solar input level should be comparable. Given the synoptic flow pattern interaction, the atmospheric pollution is expected to be most serious in PRD in autumn (Zhang et al., 2007;Li et al., 2014a). The measurement in Guangzhou was performed in late October to represent the photochemical polluted period. However, the latitude is lowest (23.1 °N), which can partly compensate the seasonal effect. The maximum of 1-h averaged O_3 concentrations were more than 100 ppbv in Shanghai, Beijing, Guangzhou, but only 79 ppbv in Chongqing, which

20 demonstrated a separation between the two classes of cities.

2.2 instrumentation

In all sites, similar instrumentations were deployed as a standard super site. All Thermo instruments were carefully maintained and calibrated during the campaigns. Only a brief description of the measurement techniques is presented. Ozone was measured by UV absorption method using the Thermo O_3 analyzer (Model 49i). The NO_2 measurement was performed by the chemiluminescence

25 after chemical conversion to NO. CO was measured by the infrared absorption technique using Thermo instrument (Model 20). Speciated VOCs measurement was performed by the GC-MS/FID. The photolysis frequencies were measured by spectrum radiometer. Meteorological parameters were measured simultaneously, e.g. ambient temperature, pressure, and relative humidity.

2.3 The model

A box model based on the Regional Atmospheric Chemical Mechanism version 2 (Goliff et al., 2013) to simulate the concentrations

30 of the short-lived OH, HO_2 and RO_2 radicals and other unmeasured secondary species. The newly proposed isoprene mechanisms are also incorporated (Peeters et al., 2014;Fuchs et al., 2013). The model was constrained to the observation of photolysis frequencies, long-lived trace gases (NO, NO_2, O_3, CO, C_2-C_{12} VOCs), and meteorological parameters. Since nitrous acid (HONO) was not measured in these campaigns, it was fixed to 2% of the observed NO_2 concentrations because good correlation was found between HONO and NO_2 in different field studies with a constant ratio being 0.02 (Elshorbany et al., 2012). The uncertainty of

35 such parameterization is discussed in section 3.3.2. The uncertainty of the model calculations depends on the model constraints

and the reaction rate constants. Taking into account the uncertainties of both measurements and kinetic rate constants, the model calculations is approximately 40% (Tan et al., 2017).

3. Results

3.1 Overview of measurements

5 The mean diurnal profiles of measured ambient temperature, $j(O^1D)$, and CO, O_3 ($O_x = O_3+NO_2$), $NO_x(=NO+NO_2)$, and AHC concentrations are shown in Fig. 2 (the time series are shown in Fig. S1-S4). The ambient temperature is relatively similar in Beijing, Shanghai, and Chongqing, but lower in Guangzhou because the campaign was conducted in a later time of a year. Similarly, the photolysis frequencies are smaller in Guangzhou. However, $j(O^1D)$ is highest in Beijing and are comparable in Shanghai and Chongqing. However, diurnal maximum O_3 concentrations are highest in Shanghai (80 ppbv) followed by Beijing (72 ppbv),

10 Guangzhou (65 ppbv), and Chongqing (56 ppbv). The diurnal peak of O_3 appears at 15:00~16:00 LT in Beijing, Guangzhou, and Chongqing. In Shanghai, the peak of O_3 shows up at 13:00 LT due to the fast increase in the morning. During the measurement period, the observed ozone concentrations exceed the Chinese National Air Quality Standard Grade II (99.3 ppbv) in Beijing, Shanghai, and Guangzhou (Table 1). When a measurement site is close to NO_x emission sources, part of the O_3 is titrated to NO_2 by fresh emitted NO. Although O_3 is regenerated in a few minutes to half hour after the photolysis of NO_2, O_3 is stored temporally

15 in the form of NO_2. Therefore, O_x, the sum of O_3 and NO_2, is a better metric to describe ozone pollution in the urban area. O_x concentrations are also shown with broken lines in Fig. 2. In this case, the O_x mean diurnal profiles in Beijing, Shanghai and Guangzhou show maximum values of about 90 ppbv (1-hour resolution), indicating the ozone pollution are comparable in these cities during the measurement period. In Chongqing, the maximum of the diurnal average is 66 ppbv. The ozone pollution is serious in autumn in Guangzhou due to the unique synoptic system, including the surface high-pressure system, hurricane movement and

20 the sea-land breeze (Fan et al., 2008). In Shanghai, the synoptic weather is crucial to pollution accumulation, and the ozone concentrations are reduced in August and September due to the cleaning effect by the summer Monsoon (Dufour et al., 2010;Geng et al., 2015).

The ozone precursors, NO_x, and AVOCs are shown in Fig. 2. In all cases, the NO_x concentrations show a typical diurnal profile with a minimum in the afternoon. In the morning, the peak is caused by the transportation emission during the rush hours. In

25 Shanghai, the nighttime NO_x concentrations also decrease after sunset but increase after midnight, which anti-correlates with the O_3. The AVOCs concentrations show similar diurnal profiles as those of NO_x, which suggests both AVOCs and NOx are originated from the same sources, e.g. traffic emission and/or manipulated by the same factor, e.g. boundary layer development. CO is also a precursor of ozone. The diurnal profiles of CO are almost flat due to their long lifetime versus OH. A small peak appears in the morning rush hours due to poor dilution condition and enhanced emission from transportation.

30 **3.2 OH reactivity and composition**

OH reactivity (k_{OH}) represents the pseudo first-order reaction rate constant of OH radical. It is a measure of the sum of sink terms due to OH radical reactants X_i, which depends on their ambient concentration $[X_i]$ and their rate coefficient with OH radical. Mathematically, k_{OH} equals to the inverse of ambient OH radical lifetime. The use of OH reactivity is of importance to understand the OH consumption potential.

35 The mean diurnal profiles of OH reactivity calculated from a box model are presented in Fig. 3, including the contribution from CO, NO_x, VOCs, and model generated secondary species. In general, the OH reactivity is lowest in the afternoon and highest in the morning rush hours due to the change of dilution condition over a day.

Atmospheric
Chemistry
and Physics
Discussions

The total OH reactivity can be measured directly with three techniques (Fuchs et al., 2017). In China, OH reactivity measurements were performed in NCP and PRD, showing large seasonal and spatial variation. In Beijing, k_{OH} measurements were conducted in an urban and suburban site during summer (Lu et al., 2013;Williams et al., 2016;Yang et al., 2017). The OH reactivity was on average in the range of 10 to 30 s^{-1} and showed large daily variation due to the meteorology changes. In PRD, OH reactivity was

5 measured in a rural site (Backgarden) in summer and suburban site (Heshan) in autumn, both of which were close to Guangzhou (<100km). In Backgarden, the average OH reactivity was in the range of 20 to 50 s^{-1} with a large contribution from isoprene (Lou et al., 2010). In Heshan, downwind of Guangzhou, OH reactivity was dominated by anthropogenic species. However, the averaged k_{OH} was comparable in two sites (Tan et al., 2018a).

In this study, the modeled OH reactivity in Guangzhou is highest (20-30 s^{-1}) among all the cities (Fig. 3), indicating a strong

10 influence of anthropogenic emission in Guangzhou. In Beijing and Chongqing, OH reactivity is comparable, in the range of 15 to 25 s^{-1}. In Chengdu, another big city in southwestern China, the modeled OH reactivity was also found to be in the range of 15 to 30 s^{-1} at three urban sites, with an exception that large OH reactivity was contributed by alkenes due to petrochemical complex industry (Tan et al., 2018b). In Shanghai, the OH reactivity was lowest (<15 s^{-1}) due to the small contribution from CO and NO$_x$. The speciation is clearly shown in Fig. 4. The contribution of OH reactivity was relatively similar among all cities as a typical

15 fingerprint of anthropogenic emission. NO$_x$ is the most important OH reactants that contribute 28%~35% to the total reactivity. In total, the inorganic species (CO and NO$_x$) contribute more than half of the reactivity. The measured AVOCs contribute to the total OH reactivity from 14% to 26%. In Beijing, the AVOC contribution is lowest as well as the absolute reactivity (2.3 s^{-1}). In Guangzhou, the contribution and absolute reactivity of AVOC (6 s^{-1} compared to 2~3 s^{-1} in other cities) are highest. However, isoprene is relatively small in Guangzhou (0.4 s^{-1}) due to the observation season. In comparison, isoprene reactivity is up to 1 s^{-1}

20 in Beijing and Chongqing but becomes negligible in Shanghai. The small isoprene concentration was also reported in another study (Geng et al., 2011).

The relative contributions of grouped VOCs are shown in Fig. 5. Anthropogenic VOCs are usually more important than the biogenic ones. The isoprene accounted for 15% of the measured VOC reactivity in Beijing and Chongqing. The shares of different VOCs groups are comparable with a slightly different portion of alkanes and alkenes. Aromatics become the most important VOC

25 group in Guangzhou, accounted for about half of the measured VOC reactivity, which is related to vehicle emissions and industry that produce VOC-related products (Zheng et al., 2009).

The OH reactivity concept is useful to estimate the ozone production for VOCs because it describes the VOC degradation rate initiated by OH oxidation that leads to net ozone production in the presence of NO and sunlight (see section 4.1). On the other hand, the ozone formation potentials (OFPs) are used to describe the theoretical ozone production maximum. This metric shows

30 the temporal Lagrangian evolution of O$_3$ production potential within a mixture of air that undergoes fully oxidation. The OFP of individual VOCs is calculated by the product of measured VOC concentrations and its MIR value (Carter, 2009), which are sum up later according to the VOC classification. Aromatics become dominant species in the OFPs due to their large carbon numbers and thus high MIR values. In Guangzhou, aromatics contributed up to 70% of the share of OFPs, followed by Shanghai (55%), Beijing (43%), and Chongqing (42%).

35 In comparison, the mixing ratios of different VOC are shown. It is worth noting that alkanes (including ethyne) accounted for a large fraction in the mixing ratio, their contribution to OFPs and OH reactivity was small. Therefore, they are not important in ozone formation and radical chemistry. It highlights the importance of the concept of OH reactivity and OFPs to describe photochemical processes accurately.

Atmospheric
Chemistry
and Physics
Discussions

3.3 OH-HO$_2$-RO$_2$ Radical concentrations and budget analysis

3.3.1 Concentrations

The OH, HO$_2$, and RO$_2$ concentrations are derived from box model calculations (Fig. S1-S4). The mean diurnal profiles are shown in Fig. 6. Modeled OH concentrations show distinct diurnal variation in cases. The maximum of OH means the diurnal profile is

5 largest in Beijing and Shanghai (7×10^6 cm^{-3}). The maximum is 4×10^6 cm^{-3} in Chongqing and further decrease to 2×10^6 cm^{-3} in Guangzhou. The relative change of OH maximum is consistent with the observed photolysis frequencies (Fig. 2). In fact, modeled OH concentrations show good correlation with the observed j(O^{1}D) (R=0.83, 0.93, 0.87, and 0.87 for Beijing, Shanghai, Guangzhou, and Chongqing) because OH chemistry relies on solar radiation input tightly. The OH maximum ranking is consistent with that of j(O^{1}D). The j(O^{1}D)-OH correlation slope was largest in Shanghai (3.0×10^{11} cm^{-3}s^{-1} compared to 2.0×10^{11} cm^{-3}s^{-1} in

10 the other cities) because the OH reactivity is lower and OH lifetime becomes longer. The good correlation between OH and j(O^{1}D) was found in other field campaigns conducted in China with a correlation coefficient more than 0.8 (Tan et al., 2017;Rohrer et al., 2014;Lu et al., 2013;Lu et al., 2012). However, the correlation slopes were about $(4.5 \pm 0.5) \times 10^{11}$ cm^{-3}s^{-1}, which are on average two times larger than the modeled results in this study. The larger correlation slope suggests that solar radiation converts more efficiently to radical concentrations. The different conversion factor could be due to the different chemical regimes in each location.

15 The larger factor was found in suburban and rural sites, where the air masses were more oxidized. The slope is comparable to the results obtained in urban environments where the slope was in the range of $(2-4) \times 10^{11}$ cm^{-3}s^{-1} (Holland et al., 2003;Michoud et al., 2012;Griffith et al., 2016;Whalley et al., 2018).

The peroxy radical concentrations are variable in different campaigns depending on the chemical conditions. A general feature is found in all cases that peroxy radical concentrations are suppressed in the morning. Since then, peroxy radical concentration

20 increases gradually and reach a peak at about 14:00 (two hours later than the maximum of solar radiation), because of the suppression by high NO. The peroxy radicals concentrations are highest in Chongqing with a maximum of mean diurnal profiles being 5×10^8 cm^{-3} for HO$_2$ and 7×10^8 cm^{-3} for RO$_2$. Meanwhile, the HO$_2$ and RO$_2$ concentrations are comparable in the other cities despite the difference in the solar radiation and chemical conditions. In Chongqing, the relative large VOC/NO$_x$ ratio leads to the highest peroxy radical concentration in the model, which reflects in the efficient radical recycling and ozone production.

25 #### 3.3.2 Radical budget analysis

All radical reactions are classified into four groups (initiation, termination, propagation, and thermos-equilibrium with reservoir species). The reaction turnover rate illustrates the important processes in the RO$_x$ radical reactions framework. The initiation and termination rate are shown in Fig. 7. The following radical budget analysis will focus on the daytime conditions (06:00—18:00) if no additional clarification.

30 The dominant radical sources are photolysis reactions, including HONO, O$_3$, HCHO and other carbonyl compounds. The photolysis of HONO and O$_3$ (producing O^{1}D and followed by H$_2$O reaction) produce OH radicals, which contributes 33-45% to the total primary source, P(RO$_x$). The HCHO photolysis produces HO$_2$ (14-33% of P(RO$_x$)) while the other carbonyl compounds photolyze to RO$_2$ radicals (3-6% of P(RO$_x$)). Therefore, photolysis reactions dominate the radical primary sources during daytime (58-86%). In contrast, alkenes ozonolysis is the dominant radical source during nighttime and the yields of OH, HO$_2$, and RO$_2$ radicals depend

35 on individual alkenes. The maximum of P(RO$_x$) mean diurnal profile is largest in Beijing (5 ppbv/h), followed by Shanghai (4.6 ppbv/h) and Chongqing (4.3 ppbv/h). The daytime averaged P(RO$_x$) is smaller in Shanghai due to the narrower peak of photolysis frequencies (Fig. 2) and shorter photolysis reaction time. The primary radical source is smallest in Guangzhou (3.2 ppbv/h) due to the later observation period in a year. However, the alkene ozonolysis contributed significantly to the radical sources

in Guangzhou (43% of the total primary source for daytime conditions), which could attribute to higher abundance of alkenes due to special emission inventory (see section 3.2).

Radical termination can be divided into two groups, the nitrogen-containing compounds, including HONO, HNO_3, $RONO_2$, and PAN-type species (L_N). The other pathway leads to peroxides formation result from the combination of two peroxy radicals (L_H).

5 The ratio between L_N and L_H depends on the NO_x concentrations. In urban environments, the limiting factor for radical propagation is the abundance of VOCs. In our case, the radical termination is dominated by L_N (>70%). Among all, the nitric acid formation was the major contributor to the radical termination in all cities (>50%). In Chongqing, the peroxide formation path contributes 26% to the radical termination, especially the ratio increase to 32% during the afternoon due to the higher VOC/NO_x ratio. Net PAN-type species formation as a radical loss becomes relatively important in Guangzhou (about 20%) due to the lower temperature

10 (Fig. 2). It is reported that on average 25% of the radical can be lost via forming PAN-type species in Beijing during winter (Tan et al., 2018c). Besides, PAN-type species formation becomes important in the urban area, e.g. it contributes 30% to the total radical loss in London downtown area (Whalley et al., 2018).

The comparison of the four cities is clearly shown in Fig. 8. The HONO photolysis is the dominant OH source in all cities except in Shanghai. The O_3 photolysis is more important than HONO photolysis in Shanghai, contributing 55% to the total OH primary

15 sources and 23% of the total radical sources. In all cities, the primary production of HO_2 is comparable to that of OH, which is mainly contributed by the HCHO photolysis and alkene ozonolysis. These results are consistent with the model calculation performed in Beijing (Yang et al., 2018) and Hong Kong (Xue et al., 2016). The importance of HONO and HCHO photolysis to radical primary production is also found in suburban and rural environments (Lu et al., 2012;Lu et al., 2013;Tan et al., 2017). In the base model scenario, HONO is scaled to NO_2 measurements and the uncertainty of this assumption is further discussed

20 following. In the base model, the HONO concentrations are scaled to the observed NO_x concentration using a scaling factor 0.02 (Elshorbany et al., 2012). In this study, we use this scaling factor between HONO and NO_x to simplify the discussion of unknown HONO sources. In the original RACM2 model, only homogenous source is included, i.e. OH+NO→HONO, which is not sufficient to support the high daytime HONO concentrations and, as a result, leads to a strong underestimation of OH concentrations (Su et al., 2011;Yang et al., 2014;Tong et al., 2016;Ye et al., 2016;Li et al., 2012;Li et al., 2014b). To evaluate the impact of missing

25 HONO source on the radical chemistry, we switched off the scaling between HONO and NO_x in a sensitivity test. Therefore, the results show that OH concentrations reduce by about 20% if the only homogenous source is considered. The modeled HO_2 and RO_2 concentrations are also reduced correspondingly (15-20%).

The RO_2 source strength is in the range of 0.2 to 0.3 ppbv/h, which is balanced by the RO_2 loss via organic nitrate formation ($RONO_2$). Therefore, the imbalance between primary source and termination of HO_2 (P>D) results in a net flow from HO_2 to OH.

30 Since the sum of RO_x initiation and termination rate should be balanced, the excess HO_2 radical production leads to the large formation of nitric acid through the net flow from HO_2 to OH. The equilibrium between RCO_3 (acetyl peroxy radicals) and PAN-types species tends to result in a radical loss (0.1~0.3 ppbv/h). The equilibrium between HO_2 and HNO_4 is fast with null effect on the radical budget.

The OH reacts with VOCs or CO and produces peroxy radicals. The peroxy radicals react with NO producing NO_2, which lead the

35 net production of O_3 in the presence of sunlight (see section 4.1). Nitric acid can be formed from the reaction between NO_2 and OH, which is an important precursor of fine particles (see 4.2). Therefore, the efficient radical propagation facilitates the secondary pollution formation.

In addition, the radical propagation between OH, HO_2, RO_2, RCO_3 are also shown in the inner part of Fig. 8. In RACM2, RCO_3 is mainly produced in the reaction between OH radical and aldehydes. RCO_3 is separated from the sum of RO_2 family and explicitly

shown in the radical propagation because RCO_3 reacts with NO and converts to RO_2. In the sum of RO_2 concentrations, RCO_3 is considered as a subgroup of RO_2 radicals (e.g. Fig. 6).

The OH reactions with CO and VOC produce to HO_2 and RO_2, respectively. The conversion from OH to RO_2 is slightly faster than OH to HO_2. In addition, the conversion from OH to RCO_3 is about one-third of the rate from OH to RO_2. In the presence of NO,

5 OH is regenerated from peroxy radicals and ozone is produced in the same process (see section 3.5). The flow rate from RO_2 to HO_2 is less than half of the flow rate from HO_2 to OH. Even considering the contribution from RCO_3+NO, RO_2 (+RCO_3) contributes less than half of the $P(O_3)$. Surprisingly, the HO_2 contribution to the total ozone production is constant at 63% in all cases. In this study, we find that the ratio between $P(O_3)$ and $k_{voc}\times[OH]$ is rather constant in the range of 1.5 to 1.6. Therefore, the robust relation between OH oxidation and ozone production indicates that it would be justified to estimate the ozone production

10 rate using the reaction rate of OH+VOC (CO) in the future. However, the nature of such a robust relation need to be investigated before real application.

4. Discussion

4.1 Ozone production and sensitivity

4.1.1 Local ozone production

15 Ozone is generated from the NO_2 photolysis, which produces NO simultaneously. The removal of NO without consuming O_3 leads to net ozone production. In the photochemical system, peroxy radicals (HO_2 and RO_2) are the major NO consumers in all photochemical reactions.

In this study, the ozone formation rate $F(O_3)$ is calculated from the NO oxidation rate by HO_2 and RO_2 radicals as denoted in E2.

$$F(O_3) = k_{HO_2+NO} \cdot HO_2 \cdot NO + k_{(RO_2+NO)eff} \cdot RO_2 \cdot NO \qquad (E2)$$

20 The chemical loss of O_3 includes O_3 photolysis (producing O^1D followed by H_2O reaction) and its reactions with alkenes, OH, HO_2 (E3). Since NO_2 can be regarded as a reservoir species of O_3, the reaction between NO_2 and OH is also considered as ozone chemical loss. In fact, the use of O_x is helpful to avoid the interruption of NO titration due to fresh emission, which is conservative to describe the ozone concentration change due to photochemical reactions (Liu, 1977).

$$D(O_3) = [O^1D][H_2O] + (k_{O_3+OH}[OH] + k_{O_3+HO_2}[HO_2] + k_{O_3+alkenes}[alkenes])[O_3] + k_{OH+NO_2}[OH][NO_2] \qquad (E3)$$

25 Therefore, the net ozone production rate $P(O_3)$ is determined by the difference between E2 and E3. The mean diurnal profiles of $P(O_3)$ are shown in Fig. 9. The ozone production rate is highest in Beijing and Shanghai with a diurnal averaged maximum reaching 19 ppbv/h. Although the peroxy radical concentrations are highest in Chongqing, the ozone production rate only shows a board peak at 13 ppbv/h. The duration of ozone production is different with the longest duration in Beijing (13 hours). Therefore, the daily integrated ozone production rate is largest in Beijing (136 ppbv). For comparison, the integrated ozone production rate were

30 92, 40, and 105 ppbv in Shanghai, Guangzhou, and Chongqing, respectively.

The O_x concentration change depends on both the local production and physical processes (E4). $R(O_3)$ represents the combined effect of all physical processes, including horizontal transportation, vertical mixing, deposition and so on.

$$\frac{d(O_x)}{d(t)} = P(O_3) + R(O_3) \qquad (E4)$$

As shown in Fig. 9, the O_x concentration changes are derived from the derivative of observed O_x concentrations. In Beijing,

35 Guangzhou, and Chongqing, the $d(O_x)/dt$ show similar increasing trends in the morning starting at 06:00 (Fig. 9). In Shanghai, positive derivative shows up at 05:00, one hour earlier than the other three cities. Also, the increase rate is fastest in Shanghai

during the morning hours. However, $d(O_x)/dt$ turn sharply from positive to negative at 12:00 in Shanghai. While positive $d(O_x)/dt$ last until 16:00 in the other three cities. The difference in the $d(O_x)/dt$ results in an early O_x peak (around noon time) in Shanghai. In the bottom panel of Fig. 9, the difference between $d(O_x)/dt$ and $P(O_3)$ are shown, which denotes the local transportation of O_x (positive: inflow; negative: outflow). In Beijing and Chongqing, the local production rate is larger than the O_x concentration increase. Hence, it suggests that the photochemical produced O_x at the measurement site is transported to downwind regions. In Shanghai and Guangzhou, both positive and negative values appear during daytime, indicating the local ozone budget changes from importation to exportation. In the morning, the increases in O_x concentrations are larger than the local ozone production rate, which is supported by additional O_x import from the volume outside. The O_x is most likely entrained from the air aloft because the raising up boundary layer mixes in the air mass aloft from the residual layer, which maintains the high load of O_x that produced from the last day and then isolated from the surface layer. Especially in Shanghai, the fast O_x concentration increase before 08:00 is mainly caused by transportation given the relatively small local production rate. The O_x import stops at about 10:00 and the surface layer becomes a net O_x source region. The O_x importation also stops in the later time of a day (at about 14:00) in Guangzhou. The O_x transportation to downwind areas (negative $R(O_3)$) are observed in Beijing, Shanghai, and Chongqing during the afternoon, and in Guangzhou after sunset, which suggest the city centers are important for O_x formation in a regional scale.

4.1.2 O_3-NO_x-VOC sensitivity

The OH-HO$_2$-RO$_2$ radical budget is useful to diagnose the O_3-NO_x-VOC sensitivity as discussed in section 3.3.2. In this section, we use the ratio of nitrate formation rate (L_N) to total radical production/termination rate (Q), known as L_N/Q ratio to evaluate the ozone production sensitivity as suggested by Kleinman et al. (1997). The threshold is 0.5 of the L_N/Q ratio. When L_N/Q is greater than 0.5, the radical termination is outweighed by the nitrate formation which indicates the ozone production is in limited to VOCs abundance; On the other hand, when L_N/Q is less than 0.5, peroxy radicals self-combination dominates radical termination indicating ozone production is under NO_x-limited control. In the radical budget analysis, we found the L_N contributed more than 70% to the radical termination in all cities. With a larger than 0.5 L_N/Q ratio, ozone production was in VOC-limited regime, which persist in all the cities in this study.

The Relative Incremental Reactivity (RIR) method is also used to evaluate the O_3-NO_x-VOC sensitivity. RIR is a useful metric for ozone sensitivity to individual precursors. The model input parameters are changed by a certain amount and the corresponding ozone concentration change is compared and summarized to reveal the O_3-NO_x-VOC sensitivity. The calculation of RIR is expressed in E5.

$$RIR(X) = \frac{\Delta O_3(X)/O_3}{\Delta C(X)/C(X)} \qquad （E5）$$

In equation 1, X represents a set of primary pollutants and O_3 represents the modeled O_3 concentrations in the base case. $\Delta C(X)/C(X)$ represents the relative change in the primary pollutants in one of the sensitivity tests. As a result, the relative change in modeled ozone concentrations is given by $\Delta O_3(X)/O_3$.

As shown in Fig. 10, the RIR values are calculated for NO_x, AHC, NHC, and CO, respectively. The AHC has the highest RIR (> 1 %/%) in all cities because ozone production is limited to the abundance of VOC in urban areas. In comparison, the RIR of NHC and CO are small (< 0.2 %/%), which demonstrates isoprene and CO are not important ozone precursors in all cities. For NO_x, the RIR values are negative indicating the ozone production is in NO_x-titration regime and thus reducing NO_x could lead to increase in O_x concentrations. It can be explained from the respect of radical budget that the OH+NO$_2$ reaction rate is a dominant part of the radical termination in all cities (Fig. 7). If the radical termination is reduced, the OH-HO$_2$-RO$_2$ radical propagation will become more efficient and thus the modeled radical concentrations will increase. One should keep in mind that HONO is scaled

to NO_2 in our base model. The reduction in NO_2 also leads to a reduction in HONO, which means less primary radical sources. Therefore, less ozone will be produced from the radical recycling, which compensates for the titration effect partly. We performed further sensitivity study that HONO is free running. The results show that the negative effect becomes more significant compared to the base model scenario (Fig. S5). In comparison, a small negative effect showed up in the RIR analysis in the base model run.

5　It is because the HONO photolysis only contributed about 40% to the primary source, smaller than the portion of $OH+NO_2$ to the termination. In another word, if HONO is

As discussed above, VOCs emission control is critical to ozone pollution reduction. To perform accurate VOC mitigation for O_3 pollution control, the AHC is further split into alkanes, alkenes, and aromatics. As shown in section 3.2, alkenes and aromatics are the dominant VOC groups with respect to OH reactivity. The RIR analysis also showed that reduction in alkenes and aromatics

10　are important for ozone pollution control in these megacities (Fig. 10). Xue et al. (2014) compared the observation in four cities (Beijing, Shanghai, Guangzhou, and Lanzhou) but located in downwind suburban areas. The results showed that ozone increase could be attributed to local ozone production in Shanghai, Guangzhou, and Lanzhou (Xue et al., 2014). Besides, ozone production was in VOC-limited regime in Shanghai and Guangzhou, among which aromatics were the most important contributor. A comparison of two megacities in China (Shanghai and Tianjin) showed that the ozone production is highly variable depending on

15　the VOC speciation at certain NO_x concentrations (Ran et al., 2012). Alkenes were important ozone precursors in Tianjin, while in Shanghai, aromatics dominated the ozone production. Based on a one-year measurement in Nanjing (YRD), the ozone production was in the VOC-limited regime and the Nanjing-Shanghai axis with its city clusters in between was subjected to a regional photochemical pollution (Ding et al., 2013). The regional model (WRF-Chem) also showed ozone production was under strong VOC-limited not only in urban but a larger regional area (Tie et al., 2013). The PRD region has been well studied from field

20　campaigns, emission inventories, and regional modeling (Zhang et al., 2008a;Zheng et al., 2009;Ding et al., 2004). The results showed both urban (Guangzhou) and downwind rural site (Xinken) were under the VOC-limited regime and negative RIR values for NO_x were found (Zhang et al., 2008b). Meanwhile, the ozone-NO_x-VOC sensitivity was found to be VOC-limited in Chongqing and the traffic emission contributed 44% to the VOCs in an urban area (Su et al., 2018;Li et al., 2018b).

4.2 Nitrate production potential

25　Nitric acid is one of the major products generated by the radical system for high NO_x conditions, which is an important precursor of particulate nitrate (NO_3^-). Nitrate has become a significant portion in particles in Beijing, Shanghai, and Nanjing (YRD) during summertime (Li et al., 2018a). The gas phase nitric acid HNO_3 together with ammonium NH_3 form a gas-particle partitioning equilibrium with NH_4NO_3 (R3), which depends on the relative humidity, temperature, and the aerosol contents (Seinfeld and Pandis, 2016).

30　$$NH_3 + HNO_3 \leftrightarrow NH_4NO_3 \qquad\qquad (R3)$$
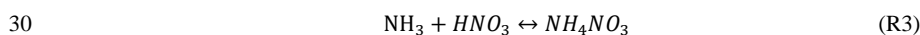
The gas-particle partitioning is calculated by the aerosol thermodynamic model (ISORROPIA). The partition is assumed to reach equilibrium because the time scale of reaching equilibrium is in range of minutes, 1-2 orders smaller than those of deposition and chemical production (Morino et al., 2006;Neuman et al., 2003). Therefore, the photochemical produced HNO_3 will deposit on to the aerosol if the ambient NH_3 is sufficient. The nitric acid could also lose via deposition. The decomposition rate is set to be

35　7 cm s^{-1}, which results in a deposition timescale being 8 hours by assuming the boundary layer height to be 2 km (typical values for summertime). The total ammonia (NH_4TOT) is calculated from an iterative method for each case to reproduce the gas-phase NH_3 concentrations reported by Pan et al. (2018). From the field measurements, the averaged NH_3 concentrations were Beijing: 16.3 µg/m^3, Shanghai: 14.6 µg/m^3 (the number is adapted from a close-by city Nanjing), Guangzhou: 5.9 µg/m^3, and Chongqing: 10.5 µg/m^3 (the number is adapted from a close-by city Chengdu) (Pan et al., 2018).

The modeled nitrate concentration and partitioning in Beijing are shown to illustrate the typical pattern of particulate nitrate formation (Fig. 11a). The total nitrate maximizes in the late afternoon while the particulate nitrate shows a board peak at night, which is mainly driven by the stronger gas-to-particle partitioning due to higher RH. Since deliquesce relative humidity (DRH) of NH_4NO_3 is about 60% in all cases, the partitioning changed dramatically with the relative humidity above DRH (nighttime) and

5   below DRH (daytime).

To investigate the nitrate concentration dependence on the nitrate production rate and ambient ammonia concentrations, the averaged nitrate concentrations are plotted as a function of daily integrated nitric acid production rate and total ammonium $(NH_4^+{}_{(a)}+NH_{3(g)})$ concentrations. As shown in Fig. 11b, the isopleth diagrams are split into two parts by the dashed line to represent the nitrate- (upper left) and ammonium-sensitive (lower right) regimes. However, the threshold for nitrate- and the ammonium-

10   sensitive regime is not distinct in the small chemical range. Actually, the nitrate concentrations are sensitive to both precursors. The daily integrated nitrate production rate and averaged total ammonium concentrations for each city are denoted by the circles (Fig. 11b). The circles are located above the ridgeline, which means nitrate concentrations are more sensitive to the change of nitrate production rate. In comparison, the averaged nitrate concentrations derived from the time-dependent calculations (as shown in Fig 11a) are 64±7, 27±8, 16±4, and 20±4 µg/m³ per day in Beijing, Shanghai, Guangzhou, and Chongqing, respectively. These

15   numbers are consistent with the EKMA plot (Fig. 11b), which indicates the results are reasonable.

In the base scenario, the other chemical compositions are set to zero (total SO_4^{2-}, Na^+, and Cl^-). The simplification uncertainty is evaluated by the following sensitivity tests. As shown in Table 2, the NH_4NO_3 concentration and the particulate nitrate to total nitrate ratio $\varepsilon(NO_3^-)$ is calculated for different model scenarios. First, if NH_3 concentrations are changed by a factor of 2, the change to partitioning is relatively small in Beijing because the NH_3 concentrations are high. It's worth noting that NH_4NO_3 concentration

20   is still high even if the NH_3 concentration is reduced by two-fold in Beijing, which highlights the difficulty in particulate nitrate reduction. In contrast, the change almost linearly correlates with the change of NH_3 in Guangzhou during the daytime due to the limited amount of NH_3. The role of other anions and cations is investigated by setting the SO_4^{2-} and Na^+ to be 10 µg/m³, respectively. Since SO_4^{2-} reacts with NH_4^+ and thus competes with the formation of NH_4NO_3. The NH_4NO_3 formation will be limited if NH_3 is not sufficient given the NH_3 to tend to react with SO_4^{2-} before NO_3^-. The nitrate concentrations decrease by 1-3 µg/m³ when SO_4^{2-}

25   is fixed in all cities to be 10 µg/m³ during day and night (Table 2). In contrast, additional cations can neutralize more nitrates and enhance the gas-to-particle partitioning. For example, if 10 µg/m³ of Na^+ is added, stronger nitrate production is found (Table 2). It is caused by two kinds of effect. First, the stronger partitioning enhances the particulate nitrate directly. Second, the total nitrate loss is reduced by less $HNO_{3(g)}$ deposition because more nitrate remains in the particle phase.

4.3 Atmospheric oxidation capacity and secondary pollution formation

30   Atmospheric oxidation capacity is mainly contributed by OH radical which dominates the chemical removal of trace gases (e.g. CO, NO_2, VOCs). The OH reactions convert primary pollutants to oxidized products (e.g. CO_2, HNO_3, OVOCs). As shown in Fig. 12, the daytime averaged OH oxidation rate is up to 10 ppbv/h in Beijing, indicating strong oxidation capacity (daily integrated oxidation rate > 100 ppbv). The OH oxidation rate is comparable in Shanghai and Chongqing (~5 ppbv/h) and reduces to 4 ppbv/h in Guangzhou. In this study, the OH oxidation rate correlates with the strength of primary radical sources $P(RO_x)$. Actually, the

35   ratio between the radical recycling rate and the primary production rate indicates the efficiency of radical propagation (E6), also known as the radical chain length.

$$ChL = (k_{VOC} + k_{CO}) \times [OH]/P(RO_x) \qquad (E6)$$

where k_{VOC} and k_{CO} represent the reactivity of VOC and CO versus OH radical, respectively.

Atmospheric
Chemistry
and Physics
Discussions

The radical chain length is on average 2.9 ± 0.3 for all cases, which is consistent with the results (3-5) derived from radical observation in urban areas (Kanaya et al., 2008;Ren et al., 2006;Emmerson et al., 2005).

As shown in section 3.3.2, $P(RO_x)$ is highly correlated with $j(O^1D)$ because photolysis reactions dominate the RO_x primary sources. An exception happens in Guangzhou that $P(RO_x)$ decrease by a factor of 2 compared to Beijing although $j(O^1D)$ is reduced by a

5 factor of 3. It is because alkenes ozonolysis reactions increase to 0.7 ppbv/h in Guangzhou (0.2-0.3 ppbv/h for other cities) and contribute nearly half of the primary source. The reduction of $P(RO_x)$ in Guangzhou is partly compensated.

More than half of the OH oxidation rate was contributed by the reaction with VOC that produce less volatile species (OVOCs) (Fig. 12). Therefore, these oxidized compounds have the potential to contribute to the particle formation due to their low volatility (Odum et al., 1997). Besides, the oxidation of NO_2 produces HNO_3, which can contribute to the particle formation given the

10 relatively high ambient NH_3 concentrations (see in section 4.2).

O_3 is another important secondary pollutants generated from the OH-HO_2-RO_2 radical system. The averaged $P(O_3)$ is consistent with the OH oxidation rate in four cities (Fig. 12). The ratio between ozone production and radical primary production rate is used to evaluate the ozone production efficiency (OPE). In this study, the OPE is highest in Chongqing (3.6 on average) due to the relative high VOC/NO_x ratio. In contrast, OPE is only 2.2 in Guangzhou and increases to 3.4 and 3.1 in Beijing and Shanghai. In

15 comparison, the OPE was found to be in the range of 3 to 7 in other cities (Kleinman et al., 2002;Lei et al., 2008). The OPE determined in this study is in the low range compared to other cities in the US, which is due to the suppression of high NO_x conditions. Since OPE generally increases with time when a plume is transported and diluted (Kleinman et al., 2002), the ozone production becomes more efficient in the suburban areas of the megacities.

Finally, the radical inner recycling rate is on average 4-5 times larger than that of radical initiation (termination), which

20 demonstrates that the secondary pollutant formation rate (e.g. ozone, nitric acid) is enhanced by the efficient radical recycling.

5. Summary and conclusion

Secondary pollution has been increasing in the last decade in Chinese cities despite the reduction of primary pollution. Ozone and fine particle precursors (e.g. H_2SO_4, HNO_3, and ELVOCs) are generated from the radical reactions. Therefore, atmospheric oxidation capacity is the core of secondary pollution formation. In this study, we present the observation of the radical precursors

25 at four Chinese megacities during photochemical polluted seasons, namely Beijing (July), Shang (August), Guangzhou (October), and Chongqing (August). A box model is used to simulate OH, HO_2 and RO_2 concentrations. The key processes are elucidated with explicit radical budget analysis. The formation mechanism of secondary pollutants (ozone, particle precursors) is investigated with the chemical model. The major findings for this study are shown in the following:

1) The metric of OH reactivity is used to demonstrate the air pollutants burden. The modeled OH reactivity show typical diurnal

30 profiles with a maximum in the morning and minimum in the afternoon. The OH reactivity is highest in Guangzhou (20-30 s^{-1}), followed by Beijing and Chongqing (15-25 s^{-1}), and smallest in Shanghai (<15 s^{-1}). More than half of the OH reactivities are contributed by inorganic species, i.e. CO and NO_x. The measured AVOCs contribute to the total OH reactivity from 14% to 26%. In Guangzhou, the contribution and absolute reactivity (6 s^{-1} compared to 2~3 s^{-1} in other cities) are highest due to the large contribution from aromatics. The shares of different VOCs groups are comparable with slightly different contribution

35 between alkanes and alkenes (in total make up 40% of the VOC reactivity except in Guangzhou).

2) Modeled OH concentrations show distinct diurnal variation. The OH mean diurnal profile maximum is largest in Beijing and Shanghai (7×10^6 cm^{-3}) and decreases to 4×10^6 cm^{-3} in Chongqing and 2×10^6 cm^{-3} in Guangzhou. The modeled OH concentrations are correlated with the photolysis frequencies ($R^2 > 0.7$) with a correlation slope to 2.0×10^{11} cm^{-3} s^{-1}

$(3.0 \times 10^{11}$ cm^{-3} s^{-1} in Shanghai). The peroxy radicals concentrations are highest in Chongqing with a diurnal maximum of 5×10^8 cm^{-3} for HO$_2$ and 7×10^8 cm^{-3} for RO$_2$ due to the relatively high VOCs/NO$_x$ ratio.

3)   The dominant radical sources are photolysis reactions, including HONO, O$_3$, HCHO and other carbonyl compounds, among which photolysis of HONO and HCHO make up nearly half of the primary sources. The mean diurnal maximum is largest in

5   Beijing (5 ppbv/h), followed by Shanghai (4.6 ppbv/h) and Chongqing (4.3 ppbv/h), and is smallest in Guangzhou (3.2 ppbv/h) due to the later observation period in a year. However, the alkene ozonolysis contributes significantly to the radical sources in Guangzhou (43% of the total primary source for daytime conditions).

4)   The daily integrated local ozone production rate is largest in Beijing (136 ppbv) and reduced to 92, 40, 105 ppbv in Shanghai, Guangzhou, and Chongqing, respectively. The measurement site represents city center conditions, where ozone precursors are

10   fresh emitted. With the advection of fresh-emitted air mass, NO$_x$ and VOCs undergo efficient photochemical processes producing a large amount of ozone and transmitted to downwind regions. The outflow of O$_x$ is identified in Beijing, Shanghai, and Chongqing during the afternoon and in Guangzhou after sunset.

5)   Ozone production is in VOC limited in all the cities presented because the L$_N$/Q ratio is greater than 0.5. Besides, we find that the RIR values of AHC are highest in all cities compared to CO, NO$_x$, and isoprene. The speciation shows that alkanes and

15   alkenes are a major contributor to total OH reactivity except in Guangzhou. In the sense of ozone formation potential, aromatics become dominant species due to their large carbon numbers and thus high MIR value. In Guangzhou, aromatics contribute up to 70% of the share of OFPs, followed by Shanghai (55%), Beijing (43%), and Chongqing (42%). In comparison, alkanes are the major contributor to the mixing ratios but had limited impact on the ozone formation and radical chemistry. To avoid the bias in the understanding of photochemistry process, it's more proper to use the concept of OH reactivity.

20   6)   The coexistence of high OH and NO$_2$ concentrations resulted in fast nitric acid production rate. The partitioning between HNO$_3$ and NO$_3^-$ is analyzed using a thermal dynamic model (ISORROPIA2). In the presence of abundant ammonium, the photochemical produced HNO$_3$ can partition to aerosol phase efficiently under high RH conditions. The daily integrated nitrate production rates are 64±7, 27±8, 16±4, and 20±4 µg/m^3 per day in Beijing, Shanghai, Guangzhou, and Chongqing, respectively. This study demonstrates that active radical chemistry could contribute to the particle pollution.

25

Atmospheric
Chemistry
and Physics
Discussions

Reference

Carter, W. P.: Updated maximum incremental reactivity scale and hydrocarbon bin reactivities for regulatory applications, California Air Resources Board Contract, 07-339, 2009.

Chan, C. K., and Yao, X.: Air pollution in mega cities in China, Atmos. Environ., 42, 1-42, https://doi.org/10.1016/j.atmosenv.2007.09.003, 2008.

Cheng, Y., Zheng, G., Wei, C., Mu, Q., Zheng, B., Wang, Z., Gao, M., Zhang, Q., He, K., Carmichael, G., Pöschl, U., and Su, H.: Reactive nitrogen chemistry in aerosol water as a source of sulfate during haze events in China, Science Advances, 2, https://doi.org/10.1126/sciadv.1601530, 2016.

Ding, A., Wang, T., Zhao, M., Wang, T., and Li, Z. K.: Simulation of sea-land breezes and a discussion of their implications on the transport of air pollution during a multi-day ozone episode in the Pearl River Delta of China, Atmos. Environ., 38, 6737-6750, https://doi.org/10.1016/j.atmosenv.2004.09.017, 2004.

Ding, A. J., Fu, C. B., Yang, X. Q., Sun, J. N., Zheng, L. F., Xie, Y. N., Herrmann, E., Nie, W., Petäjä, T., Kerminen, V. M., and Kulmala, M.: Ozone and fine particle in the western Yangtze River Delta: an overview of 1 yr data at the SORPES station, Atmos. Chem. Phys., 13, 5813-5830, https://doi.org/10.5194/acp-13-5813-2013, 2013.

Dufour, G., Eremenko, M., Orphal, J., and Flaud, J. M.: IASI observations of seasonal and day-to-day variations of tropospheric ozone over three highly populated areas of China: Beijing, Shanghai, and Hong Kong, Atmos. Chem. Phys., 10, 3787-3801, https://doi.org/10.5194/acp-10-3787-2010, 2010.

Elshorbany, Y. F., Steil, B., Brühl, C., and Lelieveld, J.: Impact of HONO on global atmospheric chemistry calculated with an empirical parameterization in the EMAC model, Atmos. Chem. Phys., 12, 9977-10000, https://doi.org/10.5194/acp-12-9977-2012, 2012.

Emmerson, K. M., Carslaw, N., and Pilling, M. J.: Urban atmospheric chemistry during the PUMA campaign 2: Radical budgets for OH, HO2 and RO2, J. Atmos. Chem., 52, 165-183, https://doi.org/10.1007/s10874-005-1323-2, 2005.

Fan, S., Wang, B., Tesche, M., Engelmann, R., Althausen, A., Liu, J., Zhu, W., Fan, Q., Li, M., Ta, N., Song, L., and Leong, K.: Meteorological conditions and structures of atmospheric boundary layer in October 2004 over Pearl River Delta area, Atmos. Environ., 42, 6174-6186, https://doi.org/10.1016/j.atmosenv.2008.01.067, 2008.

Fuchs, H., Hofzumahaus, A., Rohrer, F., Bohn, B., Brauers, T., Dorn, H. P., Haseler, R., Holland, F., Kaminski, M., Li, X., Lu, K., Nehr, S., Tillmann, R., Wegener, R., and Wahner, A.: Experimental evidence for efficient hydroxyl radical regeneration in isoprene oxidation, Nat. Geosci., 6, 1023-1026, https://doi.org/10.1038/ngeo1964, 2013.

Fuchs, H., Tan, Z. F., Lu, K. D., Bohn, B., Broch, S., Brown, S. S., Dong, H. B., Gomm, S., Haseler, R., He, L. Y., Hofzumahaus, A., Holland, F., Li, X., Liu, Y., Lu, S. H., Min, K. E., Rohrer, F., Shao, M., Wang, B. L., Wang, M., Wu, Y. S., Zeng, L. M., Zhang, Y. S., Wahner, A., and Zhang, Y. H.: OH reactivity at a rural site (Wangdu) in the North China Plain: contributions from OH reactants and experimental OH budget, Atmos. Chem. Phys., 17, 645-661, https://doi.org/10.5194/acp-17-645-2017, 2017.

Geng, F., Tie, X., Guenther, A., Li, G., Cao, J., and Harley, P.: Effect of isoprene emissions from major forests on ozone formation in the city of Shanghai, China, Atmos. Chem. Phys., 11, 10449-10459, https://doi.org/10.5194/acp-11-10449-2011, 2011.

Geng, F., Mao, X., Zhou, M., Zhong, S., and Lenschow, D.: Multi-year ozone concentration and its spectra in Shanghai, China, Sci. Total Environ., 521-522, 135-143, https://doi.org/10.1016/j.scitotenv.2015.03.082, 2015.

Goliff, W. S., Stockwell, W. R., and Lawson, C. V.: The regional atmospheric chemistry mechanism, version 2, Atmos. Environ., 68, 174-185, https://doi.org/10.1016/j.atmosenv.2012.11.038, 2013.

Griffith, S. M., Hansen, R. F., Dusanter, S., Michoud, V., Gilman, J. B., Kuster, W. C., Veres, P. R., Graus, M., de Gouw, J. A., Roberts, J., Young, C., Washenfelder, R., Brown, S. S., Thalman, R., Waxman, E., Volkamer, R., Tsai, C., Stutz, J., Flynn, J. H., Grossberg, N., Lefer, B., Alvarez, S. L., Rappenglueck, B., Mielke, L. H., Osthoff, H. D., and Stevens, P. S.: Measurements of Hydroxyl and Hydroperoxy Radicals during CalNex-LA: Model Comparisons and Radical Budgets, J. Geophys. Res., 121, 4211-4232, https://doi.org/10.1002/2015JD024358, 2016.

Guo, S., Hu, M., Zamora, M. L., Peng, J., Shang, D., Zheng, J., Du, Z., Wu, Z., Shao, M., Zeng, L., Molina, M. J., and Zhang, R.: Elucidating severe urban haze formation in China, Proc. Natl. Acad. Sci. U.S.A., 111, 17373-17378, https://doi.org/10.1073/pnas.1419604111, 2014.

He, K. B., Yang, F. M., Ma, Y. L., Zhang, Q., Yao, X. H., Chan, C. K., Cadle, S., Chan, T., and Mulawa, P.: The characteristics of PM2.5 in Beijing, China, Atmos. Environ., 35, 4959-4970, https://doi.org/10.1016/s1352-2310(01)00301-6, 2001.

Hofzumahaus, A., Rohrer, F., Lu, K., Bohn, B., Brauers, T., Chang, C.-C., Fuchs, H., Holland, F., Kita, K., Kondo, Y., Li, X., Lou, S., Shao, M., Zeng, L., Wahner, A., and Zhang, Y.: Amplified Trace Gas Removal in the Troposphere, Science, 324, 1702-1704, https://doi.org/10.1126/science.1164566, 2009.

Holland, F., Hofzumahaus, A., Schäfer, J., Kraus, A., and Pätz, H. W.: Measurements of OH and HO2 radical concentrations and photolysis frequencies during BERLIOZ, J. Geophys. Res., 108, https://doi.org/10.1029/2001JD001393, 2003.

Huang, R. J., Zhang, Y., Bozzetti, C., Ho, K. F., Cao, J. J., Han, Y., Daellenbach, K. R., Slowik, J. G., Platt, S. M., Canonaco, F., Zotter, P., Wolf, R., Pieber, S. M., Bruns, E. A., Crippa, M., Ciarelli, G., Piazzalunga, A., Schwikowski, M., Abbaszade, G., Schnelle-Kreis, J., Zimmermann, R., An, Z., Szidat, S., Baltensperger, U., El Haddad, I., and Prevot, A. S.: High secondary aerosol contribution to particulate pollution during haze events in China, Nature, 514, 218-222, https://doi.org/10.1038/nature13774, 2014.

Kan, H., Chen, R., and Tong, S.: Ambient air pollution, climate change, and population health in China, Environ. Int., 42, 10-19, https://doi.org/10.1016/j.envint.2011.03.003, 2012.

Kanaya, Y., Fukuda, M., Akimoto, H., Takegawa, N., Komazaki, Y., Yokouchi, Y., Koike, M., and Kondo, Y.: Urban photochemistry in central Tokyo: 2. Rates and regimes of oxidant (O3 + NO2) production, J. Geophys. Res., 113, D06301, https://doi.org/10.1029/2007JD008671, 2008.

Kleinman, L. I., Daum, P. H., Lee, J. H., Lee, Y. N., Nunnermacker, L. J., Springston, S. R., Newman, L., WeinsteinLloyd, J., and Sillman, S.: Dependence of ozone production on NO and hydrocarbons in the troposphere, Geophys. Res. Lett., 24, 2299-2302, https://doi.org/10.1029/97gl02279, 1997.

Kleinman, L. I., Daum, P. H., Lee, Y. N., Nunnermacker, L. J., Springston, S. R., Weinstein-Lloyd, J., and Rudolph, J.: Ozone production efficiency in an urban area, J. Geophys. Res., 107, 12, https://doi.org/10.1029/2002jd002529, 2002.

Lei, W., Zavala, M., de Foy, B., Volkamer, R., and Molina, L. T.: Characterizing ozone production and response under different meteorological conditions in Mexico City, Atmos. Chem. Phys., 8, 7571-7581, https://doi.org/10.5194/acp-8-7571-2008, 2008.

Li, H., Zhang, Q., Zheng, B., Chen, C., Wu, N., Guo, H., Zhang, Y., Zheng, Y., Li, X., and He, K.: Nitrate-driven urban haze pollution during summertime over the North China Plain, Atmos. Chem. Phys., 18, 5293-5306, https://doi.org/10.5194/acp-18-5293-2018, 2018a.

Li, J., Lu, K., Lv, W., Li, J., Zhong, L., Ou, Y., Chen, D., Huang, X., and Zhang, Y.: Fast increasing of surface ozone concentrations in Pearl River Delta characterized by a regional air quality monitoring network during 2006-2011, J. Environ. Sci. (China), 26, 23-36, https://doi.org/10.1016/s1001-0742(13)60377-0, 2014a.

Li, J., Zhai, C., Yu, J., Liu, R., Li, Y., Zeng, L., and Xie, S.: Spatiotemporal variations of ambient volatile organic compounds and their sources in Chongqing, a mountainous megacity in China, Sci. Total Environ., 627, 1442-1452, https://doi.org/10.1016/j.scitotenv.2018.02.010, 2018b.

Li, X., Brauers, T., Haseler, R., Bohn, B., Fuchs, H., Hofzumahaus, A., Holland, F., Lou, S., Lu, K. D., Rohrer, F., Hu, M., Zeng, L. M., Zhang, Y. H., Garland, R. M., Su, H., Nowak, A., Wiedensohler, A., Takegawa, N., Shao, M., and Wahner, A.: Exploring the atmospheric chemistry of nitrous acid (HONO) at a rural site in Southern China, Atmos. Chem. Phys., 12, 1497-1513, https://doi.org/10.5194/acp-12-1497-2012, 2012.

Li, X., Rohrer, F., Hofzumahaus, A., Brauers, T., Häseler, R., Bohn, B., Broch, S., Fuchs, H., Gomm, S., and Holland, F.: Missing gas-phase source of HONO inferred from zeppelin measurements in the troposphere, Science, 344, 292-296, https://doi.org/10.1126/science.1248999, 2014b.

Liu, S. C.: Possible effects on fropospheric O 3 and OH due to No emissions, Geophys. Res. Lett., 4, 325-328, https://doi.org/10.1029/GL004i008p00325, 1977.

Lou, S., Holland, F., Rohrer, F., Lu, K., Bohn, B., Brauers, T., Chang, C. C., Fuchs, H., Haseler, R., Kita, K., Kondo, Y., Li, X., Shao, M., Zeng, L., Wahner, A., Zhang, Y., Wang, W., and Hofzumahaus, A.: Atmospheric OH reactivities in the Pearl River Delta - China in summer 2006: measurement and model results, Atmos. Chem. Phys., 10, 11243-11260, https://doi.org/10.5194/acp-10-11243-2010, 2010.

Lu, K., Guo, S., Tan, Z., Wang, H., Shang, D., Liu, Y., Li, X., Wu, Z., Hu, M., and Zhang, Y.: Exploring the Atmospheric Free Radical chemistry in China: The Self-Cleansing Capacity and the Formation of Secondary air Pollution, Natl. Sci. Rev., nwy073-nwy073, https://doi.org/10.1093/nsr/nwy073, 2018.

Lu, K. D., Rohrer, F., Holland, F., Fuchs, H., Bohn, B., Brauers, T., Chang, C. C., Haseler, R., Hu, M., Kita, K., Kondo, Y., Li, X., Lou, S. R., Nehr, S., Shao, M., Zeng, L. M., Wahner, A., Zhang, Y. H., and Hofzumahaus, A.: Observation and modelling of OH and HO2 concentrations in the Pearl River Delta 2006: a missing OH source in a VOC rich atmosphere, Atmos. Chem. Phys., 12, 1541-1569, https://doi.org/10.5194/acp-12-1541-2012, 2012.

Lu, K. D., Hofzumahaus, A., Holland, F., Bohn, B., Brauers, T., Fuchs, H., Hu, M., Haseler, R., Kita, K., Kondo, Y., Li, X., Lou, S. R., Oebel, A., Shao, M., Zeng, L. M., Wahner, A., Zhu, T., Zhang, Y. H., and Rohrer, F.: Missing OH source in a suburban environment near Beijing: observed and modelled OH and HO2 concentrations in summer 2006, Atmos. Chem. Phys., 13, 1057-1080, https://doi.org/10.5194/acp-13-1057-2013, 2013.

Michoud, V., Kukui, A., Camredon, M., Colomb, A., Borbon, A., Miet, K., Aumont, B., Beekmann, M., Durand-Jolibois, R., Perrier, S., Zapf, P., Siour, G., Ait-Helal, W., Locoge, N., Sauvage, S., Afif, C., Gros, V., Furger, M., Ancellet, G., and Doussin, J. F.: Radical budget analysis in a suburban European site during the MEGAPOLI summer field campaign, Atmos. Chem. Phys., 12, 11951-11974, https://doi.org/10.5194/acp-12-11951-2012, 2012.

Morino, Y., Kondo, Y., Takegawa, N., Miyazaki, Y., Kita, K., Komazaki, Y., Fukuda, M., Miyakawa, T., Moteki, N., and Worsnop, D.: Partitioning of HNO3 and particulate nitrate over Tokyo: Effect of vertical mixing, J. Geophys. Res., 111, D15215, https://doi.org/10.1029/2005JD006887, 2006.

Neuman, J. A., Nowak, J. B., Brock, C. A., Trainer, M., Fehsenfeld, F. C., Holloway, J. S., Hübler, G., Hudson, P. K., Murphy, D. M., Nicks, D. K., Orsini, D., Parrish, D. D., Ryerson, T. B., Sueper, D. T., Sullivan, A., and Weber, R.: Variability in ammonium nitrate formation and nitric acid depletion with altitude and location over California, J. Geophys. Res., 108, 4557, https://doi.org/doi:10.1029/2003JD003616, 2003.

Odum, J. R., Jungkamp, T. P. W., Griffin, R. J., Flagan, R. C., and Seinfeld, J. H.: The Atmospheric Aerosol-Forming Potential of Whole Gasoline Vapor, Science, 276, 96-99, https://doi.org/10.1126/science.276.5309.96, 1997.

Pan, Y., Tian, S., Zhao, Y., Zhang, L., Zhu, X., Gao, J., Huang, W., Zhou, Y., Song, Y., Zhang, Q., and Wang, Y.: Identifying Ammonia Hotspots in China Using a National Observation Network, Environ. Sci. Technol., 52, 3926-3934, https://doi.org/10.1021/acs.est.7b05235, 2018.

Peeters, J., Muller, J.-F., Stavrakou, T., and Nguyen, V. S.: Hydroxyl radical recycling in isoprene oxidation driven by hydrogen bonding and hydrogen tunneling: The upgraded LIM1 mechanism, J. Phys. Chem. A, 118, 8625-8643, https://doi.org/10.1021/jp5033146, 2014.

Ran, L., Zhao, C. S., Xu, W. Y., Han, M., Lu, X. Q., Han, S. Q., Lin, W. L., Xu, X. B., Gao, W., Yu, Q., Geng, F. H., Ma, N., Deng, Z. Z., and Chen, J.: Ozone production in summer in the megacities of Tianjin and Shanghai, China: a comparative study, Atmos. Chem. Phys., 12, 7531-7542, https://doi.org/10.5194/acp-12-7531-2012, 2012.

Ren, X., Brune, W. H., Mao, J., Mitchell, M. J., Lesher, R. L., Simpas, J. B., Metcalf, A. R., Schwab, J. J., Cai, C., Li, Y., Demerjian, K. L., Felton, H. D., Boynton, G., Adams, A., Perry, J., He, Y., Zhou, X., and Hou, J.: Behavior of OH and HO2 in the winter atmosphere in New York city, Atmos. Environ., 40, S252-S263, https://doi.org/10.1016/j.atmosenv.2005.11.073, 2006.

Rohrer, F., Lu, K., Hofzumahaus, A., Bohn, B., Brauers, T., Chang, C.-C., Fuchs, H., Haseler, R., Holland, F., Hu, M., Kita, K., Kondo, Y., Li, X., Lou, S., Oebel, A., Shao, M., Zeng, L., Zhu, T., Zhang, Y., and Wahner, A.: Maximum efficiency in the hydroxyl-radical-based self-cleansing of the troposphere, Nat. Geosci., 7, 559-563, https://doi.org/10.1038/ngeo2199, 2014.

Seinfeld, J. H., and Pandis, S. N.: Atmospheric chemistry and physics: from air pollution to climate change, John Wiley & Sons, 2016.

Su, H., Cheng, Y. F., Oswald, R., Behrendt, T., Trebs, I., Meixner, F. X., Andreae, M. O., Cheng, P., Zhang, Y., and Poschl, U.: Soil Nitrite as a Source of Atmospheric HONO and OH Radicals, Science, 333, 1616-1618, https://doi.org/10.1126/science.1207687, 2011.

Su, R., Lu, K. D., Yu, J. Y., Tan, Z. F., Jiang, M. Q., Li, J., Xie, S. D., Wu, Y. S., Zeng, L. M., Zhai, C. Z., and Zhang, Y. H.: Exploration of the formation mechanism and source attribution of ambient ozone in Chongqing with an observation-based model, Sci. China Earth Sci., 61, 23-32, https://doi.org/10.1007/s11430-017-9104-9, 2018.

Sun, Y. L., Zhuang, G. S., Ying, W., Han, L. H., Guo, J. H., Mo, D., Zhang, W. J., Wang, Z. F., and Hao, Z. P.: The air-borne particulate pollution in Beijing - concentration, composition, distribution and sources, Atmos. Environ., 38, 5991-6004, https://doi.org/10.1016/j.atmosenv.2004.07.009, 2004.

Sun, Y. L., Zhuang, G. S., Tang, A. H., Wang, Y., and An, Z. S.: Chemical characteristics of PM2.5 and PM10 in haze-fog episodes in Beijing, Environ. Sci. Technol., 40, 3148-3155, https://doi.org/10.1021/es051533g, 2006.

Tan, Z., Lu, K., Hofzumahaus, A., Fuchs, H., Bohn, B., Holland, F., Liu, Y., Rohrer, F., Shao, M., Sun, K., Wu, Y., Zeng, L., Zhang, Y., Zou, Q., Kiendler-Scharr, A., Wahner, A., and Zhang, Y.: Experimental budgets of OH, HO2 and RO2 radicals and implications for ozone formation in the Pearl River Delta in China 2014, Atmos. Chem. Phys. Discuss., 2018, 1-28, https://doi.org/10.5194/acp-2018-801, 2018a.

Tan, Z., Lu, K., Jiang, M., Su, R., Dong, H., Zeng, L., Xie, S., Tan, Q., and Zhang, Y.: Exploring ozone pollution in Chengdu, southwestern China: A case study from radical chemistry to O3-VOC-NOx sensitivity, Sci. Total Environ., 636, 775-786, https://doi.org/10.1016/j.scitotenv.2018.04.286, 2018b.

Tan, Z., Rohrer, F., Lu, K., Ma, X., Bohn, B., Broch, S., Dong, H., Fuchs, H., Gkatzelis, G. I., Hofzumahaus, A., Holland, F., Li, X., Liu, Y., Liu, Y., Novelli, A., Shao, M., Wang, H., Wu, Y., Zeng, L., Hu, M., Kiendler-Scharr, A., Wahner, A., and Zhang, Y.: Wintertime photochemistry in Beijing: observations of ROx radical concentrations in the North China Plain during the BEST-ONE campaign, Atmos. Chem. Phys., 18, 12391-12411, 10.5194/acp-18-12391-2018, 2018c.

Tan, Z. F., Fuchs, H., Lu, K. D., Hofzumahaus, A., Bohn, B., Broch, S., Dong, H. B., Gomm, S., Haseler, R., He, L. Y., Holland, F., Li, X., Liu, Y., Lu, S. H., Rohrer, F., Shao, M., Wang, B. L., Wang, M., Wu, Y. S., Zeng, L. M., Zhang, Y. S., Wahner, A., and Zhang, Y. H.: Radical chemistry at a rural site (Wangdu) in the North China Plain: observation and model calculations of OH, HO2 and RO2 radicals, Atmos. Chem. Phys., 17, 663-690, https://doi.org/10.5194/acp-17-663-2017, 2017.

Tham, Y. J., Wang, Z., Li, Q., Yun, H., Wang, W., Wang, X., Xue, L., Lu, K., Ma, N., Bohn, B., Li, X., Kecorius, S., Größ, J., Shao, M., Wiedensohler, A., Zhang, Y., and Wang, T.: Significant concentrations of nitryl chloride sustained in the morning: investigations of the causes and impacts on ozone production in a polluted region of northern China, Atmos. Chem. Phys., 16, 14959-14977, https://doi.org/10.5194/acp-16-14959-2016, 2016.

Tham, Y. J., Wang, Z., Li, Q., Wang, W., Wang, X., Lu, K., Ma, N., Yan, C., Kecorius, S., Wiedensohler, A., Zhang, Y., and Wang, T.: Heterogeneous N2O5 uptake coefficient and production yield of ClNO2 in polluted northern China: Roles of aerosol water content and chemical composition, Atmos. Chem. Phys. Discuss., 2018, 1-27, https://doi.org/10.5194/acp-2018-313, 2018.

Tie, X., Geng, F., Guenther, A., Cao, J., Greenberg, J., Zhang, R., Apel, E., Li, G., Weinheimer, A., Chen, J., and Cai, C.: Megacity impacts on regional ozone formation: observations and WRF-Chem modeling for the MIRAGE-Shanghai field campaign, Atmos. Chem. Phys., 13, 5655-5669, https://doi.org/10.5194/acp-13-5655-2013, 2013.

Tong, S., Hou, S., Zhang, Y., Chu, B., Liu, Y., He, H., Zhao, P., and Ge, M.: Exploring the nitrous acid (HONO) formation mechanism in winter Beijing: direct emissions and heterogeneous production in urban and suburban areas, Faraday Discuss., 189, 213-230, https://doi.org/10.1039/C5FD00163C, 2016.

Wang, H., Lu, K., Chen, X., Zhu, Q., Chen, Q., Guo, S., Jiang, M., Li, X., Shang, D., Tan, Z., Wu, Y., Wu, Z., Zou, Q., Zheng, Y., Zeng, L., Zhu, T., Hu, M., and Zhang, Y.: High N2O5 Concentrations Observed in Urban Beijing: Implications of a Large Nitrate Formation Pathway, Environ. Sci. Technol. Lett., https://doi.org/10.1021/acs.estlett.7b00341, 2017a.

Wang, T., Tham, Y. J., Xue, L., Li, Q., Zha, Q., Wang, Z., Poon, S. C. N., Dubé, W. P., Blake, D. R., Louie, P. K. K., Luk, C. W. Y., Tsui, W., and Brown, S. S.: Observations of nitryl chloride and modeling its source and effect on ozone in the planetary boundary layer of southern China, J. Geophys. Res., 121, 2476-2489, https://doi.org/10.1002/2015JD024556, 2016.
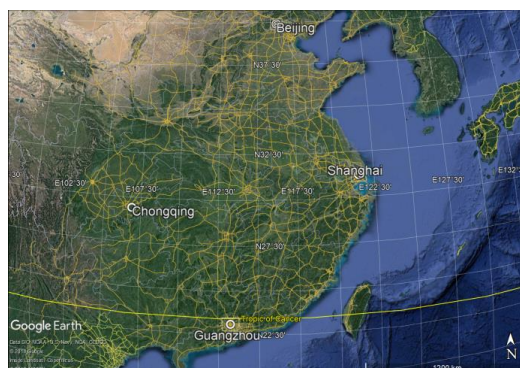
Atmospheric
Chemistry
and Physics
Discussions

Wang, X., Wang, H., Xue, L., Wang, T., Wang, L., Gu, R., Wang, W., Tham, Y. J., Wang, Z., Yang, L., Chen, J., and Wang, W.: Observations of N2O5 and ClNO2 at a polluted urban surface site in North China: High N2O5 uptake coefficients and low ClNO2 product yields, Atmos. Environ., 156, 125-134, https://doi.org/10.1016/j.atmosenv.2017.02.035, 2017b.

Wang, Z., Wang, W., Tham, Y. J., Li, Q., Wang, H., Wen, L., Wang, X., and Wang, T.: Fast heterogeneous N2O5 uptake and ClNO2 production in power plant and industrial plumes observed in the nocturnal residual layer over the North China Plain, Atmos. Chem. Phys., 17, 12361-12378, https://doi.org/10.5194/acp-17-12361-2017, 2017c.

Whalley, L. K., Stone, D., Dunmore, R., Hamilton, J., Hopkins, J. R., Lee, J. D., Lewis, A. C., Williams, P., Kleffmann, J., Laufs, S., Woodward-Massey, R., and Heard, D. E.: Understanding in situ ozone production in the summertime through radical observations and modelling studies during the Clean air for London project (ClearfLo), Atmos. Chem. Phys., 18, 2547-2571, https://doi.org/10.5194/acp-18-2547-2018, 2018.

Williams, J., Kessel, S. U., Nolscher, A. C., Yang, Y. D., Lee, Y., Yanez-Serrano, A. M., Wolff, S., Kesselmeier, J., Klupfel, T., Lelieveld, J., and Shao, M.: Opposite OH reactivity and ozone cycles in the Amazon rainforest and megacity Beijing: Subversion of biospheric oxidant control by anthropogenic emissions, Atmos. Environ., 125, 112-118, https://doi.org/10.1016/j.atmosenv.2015.11.007, 2016.

Xue, L., Gu, R., Wang, T., Wang, X., Saunders, S., Blake, D., Louie, P. K. K., Luk, C. W. Y., Simpson, I., Xu, Z., Wang, Z., Gao, Y., Lee, S., Mellouki, A., and Wang, W.: Oxidative capacity and radical chemistry in the polluted atmosphere of Hong Kong and Pearl River Delta region: analysis of a severe photochemical smog episode, Atmos. Chem. Phys., 16, 9891-9903, https://doi.org/10.5194/acp-16-9891-2016, 2016.

Xue, L. K., Wang, T., Gao, J., Ding, A. J., Zhou, X. H., Blake, D. R., Wang, X. F., Saunders, S. M., Fan, S. J., Zuo, H. C., Zhang, Q. Z., and Wang, W. X.: Ground-level ozone in four Chinese cities: precursors, regional transport and heterogeneous processes, Atmos. Chem. Phys., 14, 13175-13188, https://doi.org/10.5194/acp-14-13175-2014, 2014.

Yang, Q., Su, H., Li, X., Cheng, Y., Lu, K., Cheng, P., Gu, J., Guo, S., Hu, M., Zeng, L., Zhu, T., and Zhang, Y.: Daytime HONO formation in the suburban area of the megacity Beijing, China, Sci. China Chem., 57, 1032-1042, https://doi.org/10.1007/s11426-013-5044-0, 2014.

Yang, X., Xue, L., Wang, T., Wang, X., Gao, J., Lee, S., Blake, D. R., Chai, F., and Wang, W.: Observations and explicit modeling of summertime carbonyl formation in Beijing: Identification of key precursor species and their impact on atmospheric oxidation chemistry, J. Geophys. Res., 123, 1426-1440, https://doi.org/10.1002/2017JD027403, 2018.

Yang, Y. D., Shao, M., Kessel, S., Li, Y., Lu, K. D., Lu, S. H., Williams, J., Zhang, Y. H., Zeng, L. M., Noelscher, A. C., Wu, Y. S., Wang, X. M., and Zheng, J. Y.: How the OH reactivity affects the ozone production efficiency: case studies in Beijing and Heshan, China, Atmos. Chem. Phys., 17, 7127-7142, https://doi.org/10.5194/acp-17-7127-2017, 2017.

Ye, C. X., Zhou, X. L., Pu, D., Stutz, J., Festa, J., Spolaor, M., Tsai, C., Cantrell, C., Mauldin, R. L., Campos, T., Weinheimer, A., Hornbrook, R. S., Apel, E. C., Guenther, A., Kaser, L., Yuan, B., Karl, T., Haggerty, J., Hall, S., Ullmann, K., Smith, J. N., Ortega, J., and Knote, C.: Rapid cycling of reactive nitrogen in the marine boundary layer, Nature, 532, 489-491, https://doi.org/10.1038/nature17195, 2016.

Zhang, J., Wang, T., Chameides, W. L., Cardelino, C., Kwok, J., Blake, D. R., Ding, A., and So, K. L.: Ozone production and hydrocarbon reactivity in Hong Kong, Southern China, Atmos. Chem. Phys., 7, 557-573, https://doi.org/10.5194/acp-7-557-2007, 2007.

Zhang, Y. H., Hu, M., Zhong, L. J., Wiedensohler, A., Liu, S. C., Andreae, M. O., Wang, W., and Fan, S. J.: Regional Integrated Experiments on Air Quality over Pearl River Delta 2004 (PRIDE-PRD2004): Overview, Atmos. Environ., 42, 6157-6173, https://doi.org/10.1016/j.atmosenv.2008.03.025, 2008a.

Zhang, Y. H., Su, H., Zhong, L. J., Cheng, Y. F., Zeng, L. M., Wang, X. S., Xiang, Y. R., Wang, J. L., Gao, D. F., Shao, M., Fan, S. J., and Liu, S. C.: Regional ozone pollution and observation-based approach for analyzing ozone–precursor relationship during the PRIDE-PRD2004 campaign, Atmos. Environ., 42, 6203-6218, https://doi.org/10.1016/j.atmosenv.2008.05.002, 2008b.

Zheng, J., Shao, M., Che, W., Zhang, L., Zhong, L., Zhang, Y., and Streets, D.: Speciated VOC Emission Inventory and Spatial Patterns of Ozone Formation Potential in the Pearl River Delta, China, Environ. Sci. Technol., 43, 8580-8586, https://doi.org/10.1021/es901688e, 2009.

Zheng, M., Salmon, L. G., Schauer, J. J., Zeng, L. M., Kiang, C. S., Zhang, Y. H., and Cass, G. R.: Seasonal trends in PM2.5 source contributions in Beijing, China, Atmos. Environ., 39, 3967-3976, https://doi.org/10.1016/j.atmosenv.2005.03.036, 2005.

50

Atmospheric
Chemistry
and Physics
Discussions

Open Access

Table 1 Overview of the measurement sites.

Site	Location	Observation period	1h O_3 maximum [ppbv]
Beijing	116.42 °E, 39.92 °N	Jul. 02 — Jul. 19 2014	110
Shanghai	121.54 °E, 31.12 °N	Aug.21 —Sep. 02 2016	123
Guangzhou	113.33 °E, 23.10 °N	Oct. 23 —Oct. 31 2015	100
Chongqing	106.57 °E, 29.64 °N	Aug. 27 — Sep. 04 2015	79

5   **Table 2 Equilibrium Model sensitivity summary for NH₄NO₃ mass concentration and particulate nitrate to total nitrate ratio ε(NO₃⁻) during daytime (06:00—18:00) and nighttime (00:00—06:00, 18:00—24:00).**

	Base		NH₃×2		NH₃ / 2		SO₄²⁻=10 µg/m³		Na⁺=10 µg/m³	
	NO_3^- [µg/m³]	ε(NO_3^-) [%]	NO_3^- [µg/m³]	ε(NO_3^-) [%]	NO_3^- [µg/m³]	ε(NO_3^-) [%]	NO_3^- [µg/m³]	ε(NO_3^-) [%]	NO_3^- [µg/m³]	ε(NO_3^-) [%]
Beijing										
Day	59	83	77	92	29	58	56	81	60	83
Night	69	96	86	100	41	83	67	96	73	99
Shanghai										
Day	21	59	39	83	3	16	17	53	31	73
Night	33	92	49	99	15	69	32	91	44	98
Guangzhou										
Day	13	56	28	83	1	11	11	50	28	82
Night	21	86	34	97	5	39	19	84	32	95
Chongqing										
Day	16	57	34	83	1	7	14	53	28	76
Night	24	85	40	97	5	36	23	85	35	93

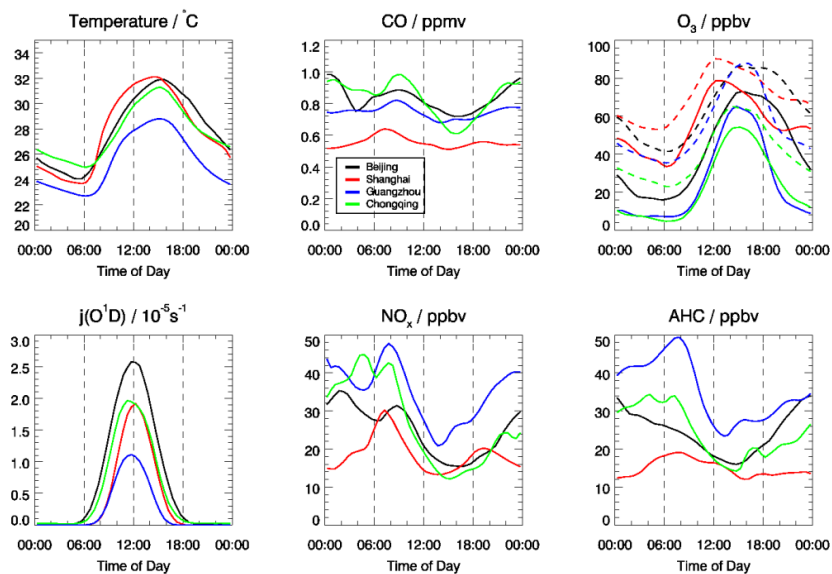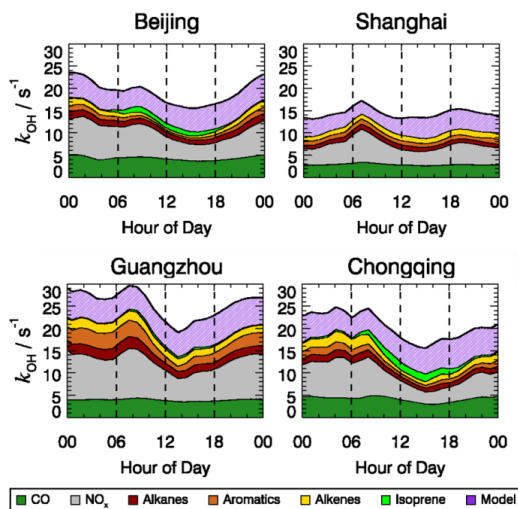10   **Figure 1. The location of the four measurement sites in Chinese megacities.**

Figure 2. Mean diurnal variation of measured temperature, CO, O₃, j(O¹D), NOₓ and Anthropogenic Volatile Organic Compounds (AHC) in four field studies. Oₓ is denoted in the same panel as O₃ with dashed lines.

5   **Figure 3. Mean diurnal profile of contributions from all measured species for OH reactivity in Beijing, Shanghai, Guangzhou, and Chengdu. The filled areas represent different atmospheric constituents.**
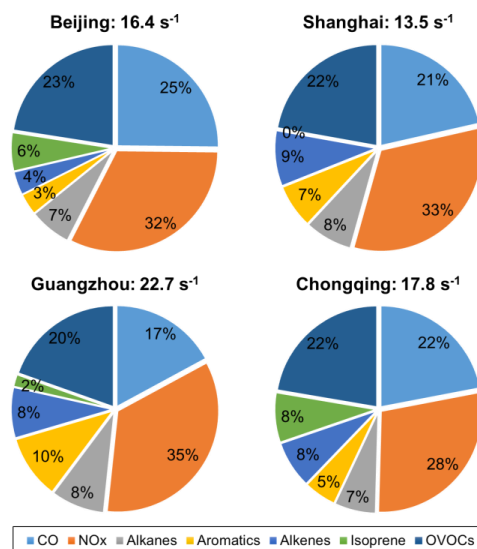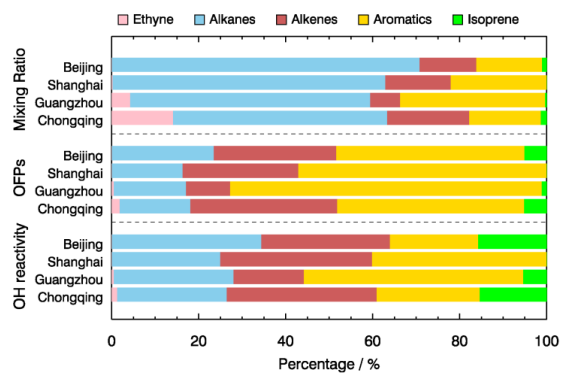
Figure 4. Contributions of different atmospheric constituents to OH reactivity in Beijing, Shanghai, Guangzhou, and Chongqing.

Figure 5. The group compositions (mixing ratios) in percentages for VOCs as well as their shares in OFPs and OH reactivity for four cities.

Atmospheric
Chemistry
and Physics
Discussions
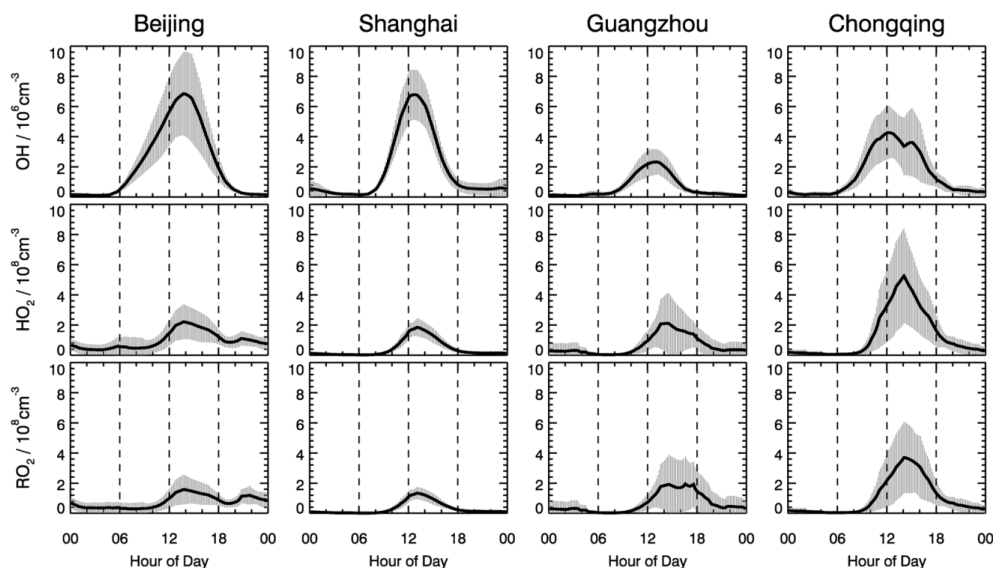
Figure 6. Mean diurnal profiles of modeled OH, HO₂, RO₂ concentrations in four measurement sites. The vertical bars denote the variability of model calculations.
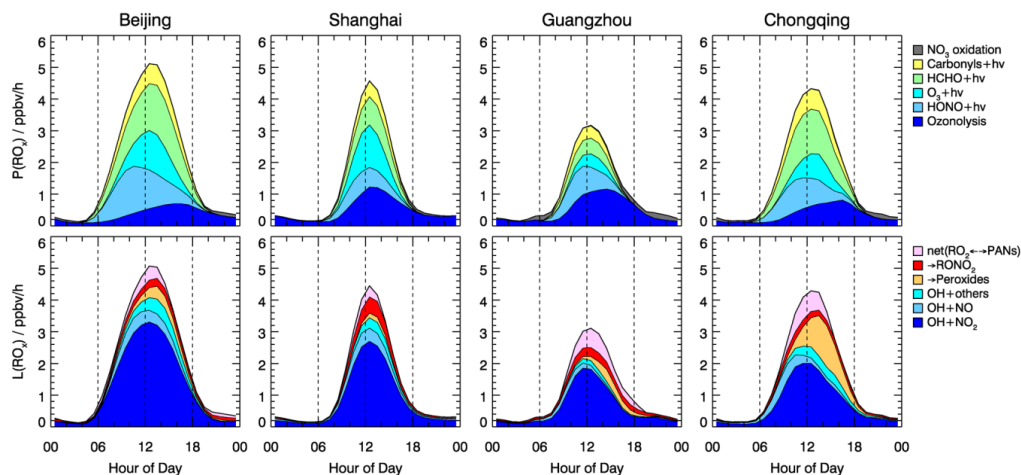
5 **Figure 7. Hourly averaged primary sources and sinks of ROₓ radicals derived from model calculations in four measurement sites.**

Atmospheric
Chemistry
and Physics
Discussions
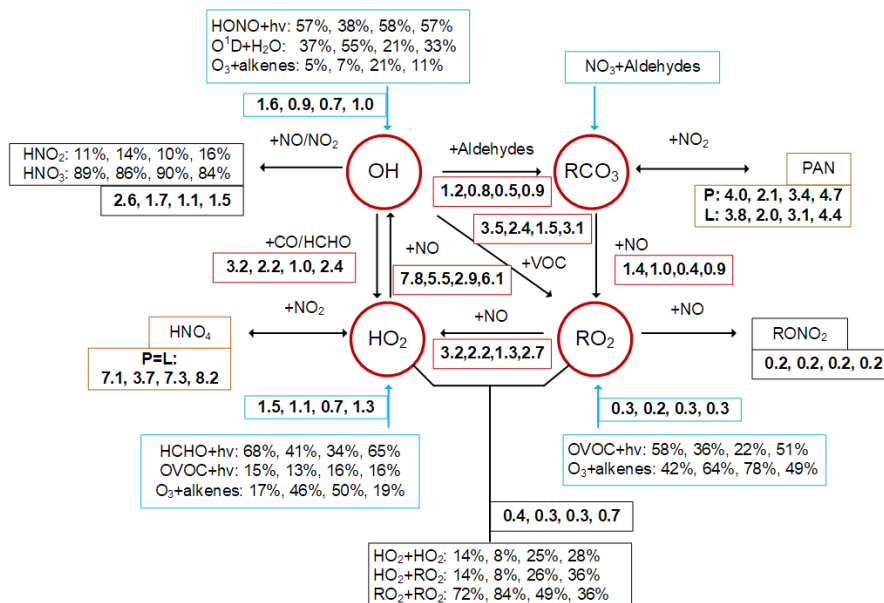
Figure 8. Comparison of OH-HO₂-RO₂ radical budget in four cities for daytime conditions (06:00-18:00). The numbers are sorted in the order of Beijing, Shanghai, Guangzhou, and Chongqing from left to right. Blue boxes denote radical primary sources, black boxes denote radical termination, red boxes denote radical propagation, and yellow boxes denote equilibrium between radicals and reservoir species.
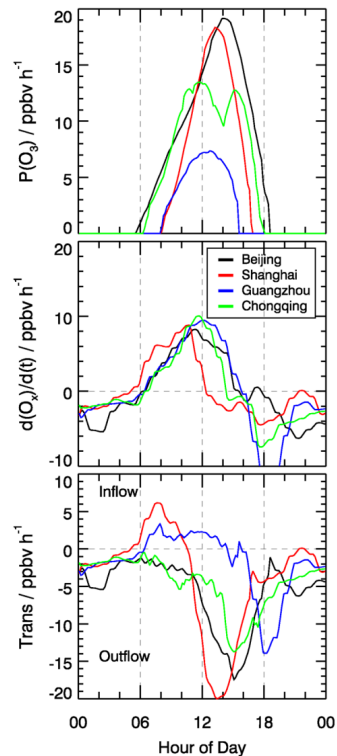
Figure 9. In situ ozone budget analysis at four cities. The upper panel denotes the local ozone production rate P(O₃) derived from model calculation. The middle panel denotes the derivatives of observed Oₓ concentrations d(Oₓ)/d(t). The bottom panel denotes the difference between P(O₃) and d(Oₓ)/d(t), which indicate the role of local chemical production on transportation (see text).
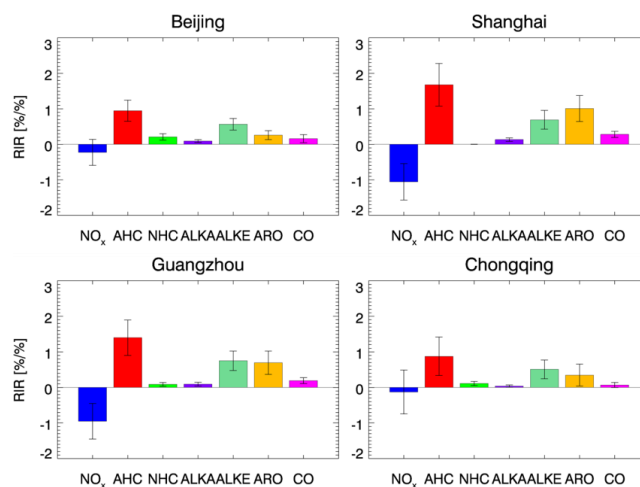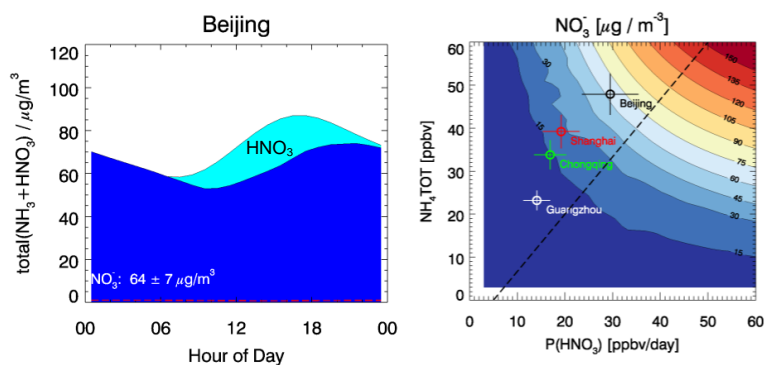
Figure 10. The RIR analysis for NOx, AHC, CO and NHC at four sites.

Figure 11. Modelled nitrate production from gas-phase oxidation. (a) The mean diurnal profile of modelled total nitrate concentration
5 **and its gas-particle partitioning. (b) Functional dependence of particulate nitrate concentrations on daily integrated nitrate production**
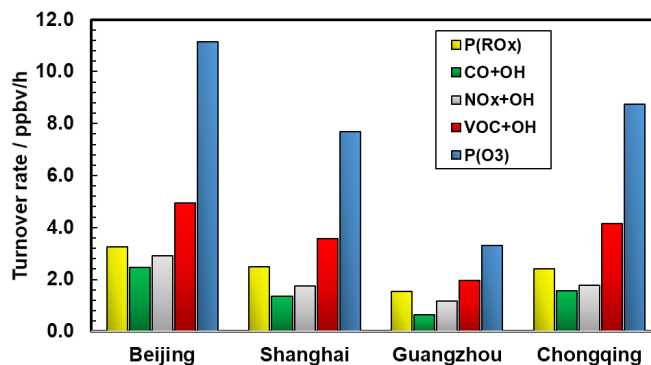**rate and total ammonium concentrations.**

Figure 12 Inter-comparison of atmospheric oxidation rate for four megacities.